International Forum on Aeroelasticity and Structural Dynamics
IFASD 2024
17-21 June 2024, The Hague, The Netherlands

T-TAIL TRANSONIC FLUTTER WIND TUNNEL TEST PART 1: SEALING SYSTEM DESIGN AND MODEL TESTING

Valentin Lanari [1], Arnaud Lepage [1], Elsa Bréus [2]

[1] ONERA
The French Aerospace Lab, 92322 Châtillon, FRANCE
valentin.lanari@onera.fr
[2] Dassault Aviation
78 quai Marcel Dassault, 92552 Saint-Cloud France

Keywords: Flutter, wind tunnel test, transonic, T-tail, aeroelasticity

Abstract: This paper presents the test setup improvements and the experimental results of the recent T-tail transonic flutter test performed at ONERA S2MA pressurized wind tunnel in November 2022. The test campaign is the culmination of flutter investigations initiated in Clean Sky 1's "Smart Fixed Wing Aircraft Integrated Technology Demonstrator" program where U-tail configurations were studied [1]. The current presented work was performed in the frame of Clean Sky 2's Airframe ITD program in partnership with Dassault Aviation.

First, the paper presents the sealing system developed to improve the test setup and tackle issues encountered in the previous 2016 test campaign. Air leakage from the fuselage at the root of the tail wing model led to unwanted aerodynamic effects, and asked for more post-processing efforts to be taken into account. Efforts were made to develop a sealing system solution involving labyrinth sealing and fine gap tuning during dynamic displacements of the test setup while keeping a healthy model dynamic behavior. The heavily instrumented model allowed the validation of the sealing solution during the wind tunnel tests without any negative impact on the aeroelastic characteristics of the T-tail model.

Then, the wind tunnel test and its associated experimental results and observations over four geometrical configurations of T-tail model are presented, with variations of yaw and dihedral angle of the horizontal stabilizer. Both steady and unsteady aerodynamics were investigated, including Mach number variations (from M=0.7 to M=0.925), forced pitch motion excitation frequency, angle of attack, and stagnation pressure variations. The remotely configurable test setup and safety system allowed a controlled investigation of aeroelastic instabilities apparition beyond flutter onset. The extensive database measured helped understanding aeroelastic instabilities occurring on a T-tail model, and permitted to confront numerical capabilities to predict flutter instabilities in transonic regimes. The numerical restitutions using high-fidelity CFD tools are presented in a companion paper [2].

1 INTRODUCTION

The global effort to reduce the environmental impact of air transport led to the study of new innovative aircraft architectures. Business jet aviation seems to head more and more towards T-tail configurations, but safety must be placed in the foreground when applying new technologies at an industry level. Extensive testing is required to generate a database for model validation with detailed comparisons between experimental results and simulations. The present paper presents the activities conducted in the framework of the Clean Sky 2's Airframe ITD program, where a successful transonic flutter test campaign on a T-tail model was completed at ONERA S2MA wind tunnel facility in December 2022. The test campaign was prepared by ONERA and Dassault Aviation and builds on previous work from Clean Sky 1 “Smart Fixed Wing Aircraft Integrated Technology Demonstrator” program where transonic flutter on U-tail configuration was investigated during a wind tunnel test that occurred in 2016.

Figure 1-1 Photo of Clean Sky 1 U-tail flutter test

The previous test from Clean Sky 1 confirmed our capabilities to perform transonic flutter test and investigate the aeroelastic instability while guaranteeing the safety of both model and facility. The idea behind the new flutter test was to keep the test setup from 2016, which proved its effectiveness with a well-known and healthy dynamic behavior, and address issues encountered in 2016 to increase the quality of the newly generated database.

First, the tail model had to be redesigned for the purpose of a T-tail study, with a geometry at the junction between the horizontal and vertical tail plane more representative of conventional aircraft. During the previous tests, complex aerodynamic effects were observed in the corner flow region in transonic regime where flow separation was observed prematurely on simulations than on the wind tunnel data. Additionally, aerodynamic interactions between the horizontal and vertical stabilizers were too strong with shocks propagating between the two planes.

Then, the other issue that had to be taken care of was the air leakage occurring at the root of the U-tail model due to the pressure differential between the test section and the other side of the wind tunnel wall. Airflow was entering the test section through the fuselage window. The flow perturbation going out of the fuselage had a stabilizing effect on flutter and complicated the numerical restitutions of the test. During the test, sealing was attempted using foam and aluminum tape to reduce the fuselage window, but none of these solutions was effective during the entire rotation, nor compatible with the dynamic motion of the model. Tests with and without fuselage window reduction showed that flutter could not be achieved without window reduction, while it was obtained with sealing. These observations directly link the air leakage with flutter sensitivity,

and the direct consequence was some discrepancies in the flutter results and extra efforts in the post-processing and restitution to take this effect into account. A sealing solution resistant to pressure differential, compatible with model dynamic motion, tunable and not impacting the test setup dynamic behavior had to be designed.

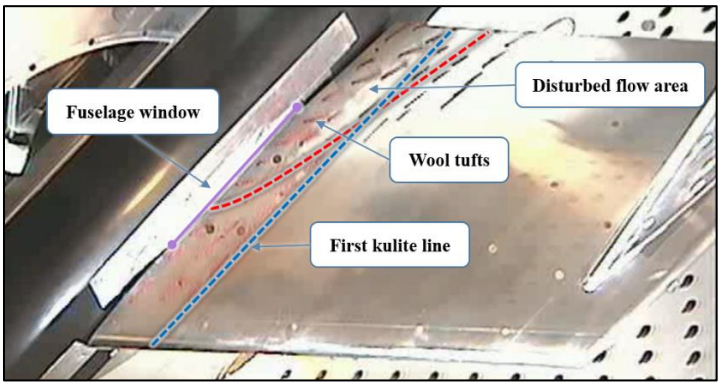

Figure 1-2 Air leakage at the root of the model identified with wool tuft at M=0.7, Pi=1bar, AoA=0°

2 TEST SETUP

2.1 Wind tunnel model dynamics

The test setup principles monitoring flutter onsets and dynamic excitations have already been presented in [1]. They are here simply reminded for a better understanding of the sealing solution designed. Classical bending and torsion modes involved in flutter are here replaced by a pitch and roll mode. However, aeroelastic principles remain the same regarding the physics behind this instability. The T-tail model has two controlled degrees of freedom, the pitch and the roll motion identified by the bearing axes shown in Figure 2-1 Flutter mechanical configurationFigure 2-1. The two mechanical configurations of the setup needed for flutter study as well as steady and unsteady aerodynamics are presented below.

2.1.1 Flutter configuration

In flutter configuration, two major flexural elements are depicted in blue in Figure 2-1. The torsion beam is attached to the shaft, and clamped at the other end by a remotely movable hydraulic actuator. The clamping length adjusts the pitch mode natural frequency and tunes the flutter domain. The S-beams act as springs that we can add or remove to adjust the roll mode natural frequency. The interaction between these two modes under specific wind tunnel conditions leads to flutter instability. A hydraulic actuator with an unbalanced mass fixed on the table serves as an additional exciter to increase the energy amount absorbed by the test setup. A safety system triggered by monitoring sensors allows starting the flutter instability, and stopping it within 0.1 s by clamping the pitch motion.

2.1.2 Pressure configuration

In pressure configuration, presented in Figure 2-2, the torsion beam is removed, and the shaft holding the T-tail model is rigidly attached to the hydraulic actuator allowing precise control over static and dynamic angle of attack variations. During the test, static incidences are first set to identify steady aerodynamic characteristics. Then, dynamic excitations of the model with variations of frequencies and amplitude allows identification of the unsteady aerodynamic behavior. In this mechanical configuration, the S-beams are bypassed by a rigid frame locking the

table position. No flutter instability can occur in this configuration since both modes participating in the phenomenon are spread apart in the frequency domain.

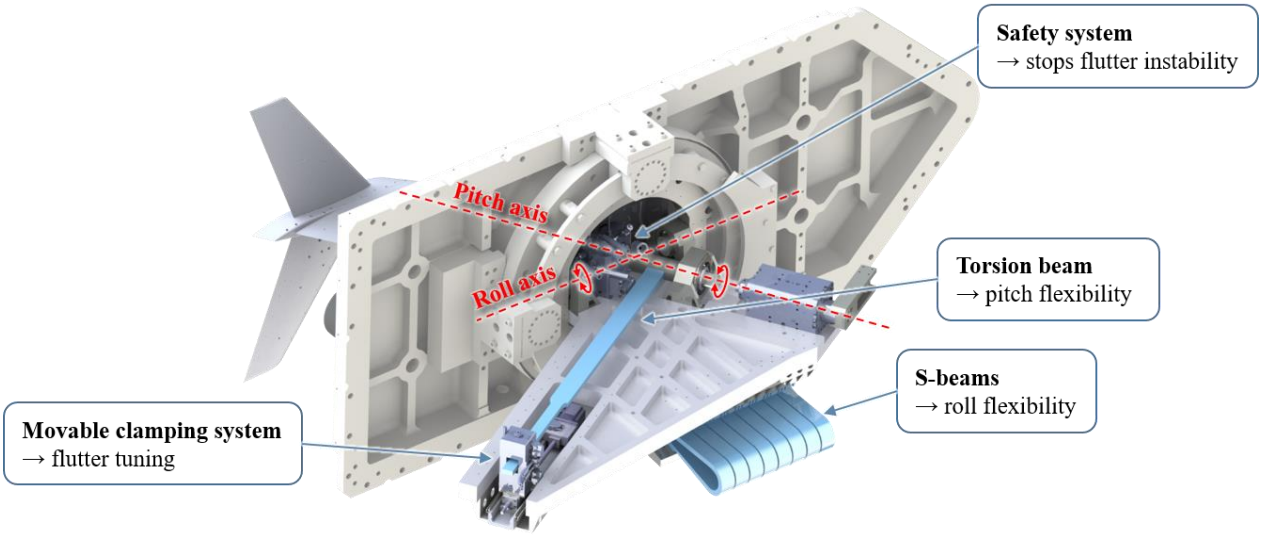

Figure 2-1 Flutter mechanical configuration

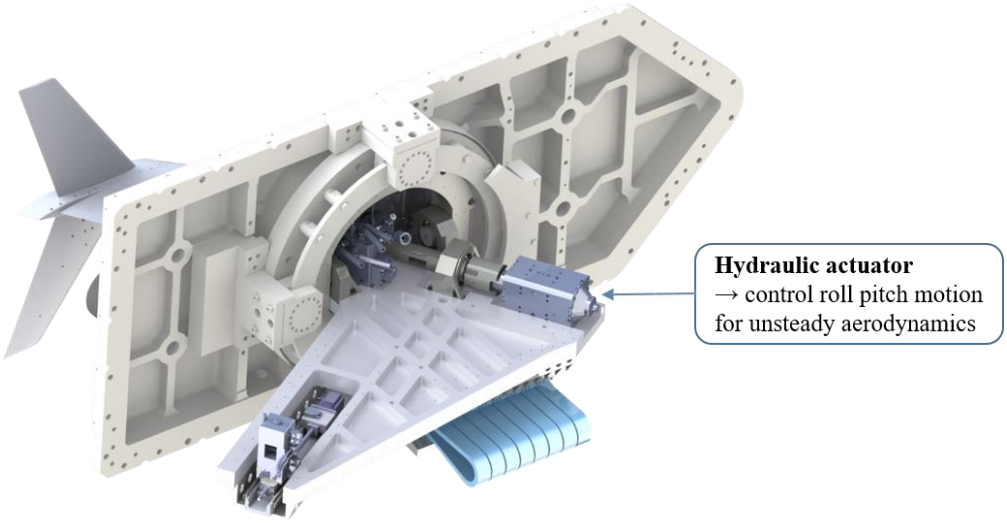

Figure 2-2 Pressure mechanical configuration

2.2 Sealing system

Since the fuselage is fixed and only the model moves thanks to the hydraulic actuator during the test, gaps are inherent of the system to leave enough room for dynamic motion of the system. To provide a "leak proof" setup allowing cleaner aerodynamics at the root of the model and to match the first objective of the test, a sealing solution had to be designed with many constraints.

- The solution must be compliant with the already existing flutter setup
- The impact of the solution on the dynamic behavior of the setup must be reduced to a minimum, meaning a small addition of mass, stiffness or damping.
- The solution must leave parts of the setup accessible for the change of mechanical configurations

- The design must be compatible with S2MA wind tunnel operating conditions

Three solutions were investigated and compared regarding their own risks and the respect of the constraints.

2.2.1 Design

The strategy of the solution is to decrease the cross-section at the wind tunnel wall, and increase the pressure drop to lower the mass flow rate of the leakage. One of the advantages of the solution is that it treats separately the two degrees of freedom of the setup.

The system is decomposed as follows:

- Sealing carter: A mobile part fixed to the table and to the bearing box, matching perfectly the shape of already existing elements. The carter is concentric with the roll axis to provide a constant distance between the external surface to the rotation axis. The sealing carter is presented in Figure 2-3 in orange.
- Labyrinth sealing: Represented in purple in Figure 2-4, see through labyrinth sealing is used to increase the pressure drop between the test section and the facility [5]. They are located on fixed parts of the sealing solution attached to the wind tunnel turret. The two lateral vertical parts and the two upper and lower cylindrical parts completely encapsulate the sealing carter. Cylindrical parts are concentric with the roll axis so that the radial gap between the carter and the labyrinth teeth stays constant. A frame going around the labyrinth sealing is designed to create contact between the sealing solution and the wind tunnel wall, and force the air to pass through the labyrinth teeth. To avoid uneven contact, rubber is stuck to the frame to ensure constant and leak proof sealing.
- Labyrinth sleeve: Represented in gray Figure 2-4, the sleeve is fixed on the front ball bearing support and concentric with the pitch axis, to avoid any leakage through the bearing. This part does not move during pitch rotation as it is not fixed on the shaft.

Degrees of freedom with adjustment screws are provided on the design to precisely adjust the labyrinth parts and have a fine-tuning of the gap between the labyrinth teeth and the carter. These degrees of freedom have been also provided for any misalignment or deformation under loads during the test campaign.

The complexity of the solution relies on the balance between small internal gaps to reduce the cross section and the leakage, and sufficient gaps to avoid contact and friction during flutter test. For the tests, the gap between the labyrinth sleeve and the shaft was 0.5 mm and the gap between the sealing carter and the labyrinth sealing was 1 mm. Openings on the wind tunnel wall have been added to ensure the accessibility of the adjustment screws in case of a contact event. An inductance sensor was used on the top and bottom labyrinth sealing parts to measure the gap variations during the test. Although this sensor gives a local information on the possible contact between parts, it is still a good information to evaluate the sealing system deformation to the pressure differential and motion. Contact strips can be used for contact identification over the entire system surface for future tests. The selected solution matches all of the initial constraints, but its impact on the natural frequencies and mode shapes of the test setup has to be evaluated. Overall, only the mass of the sealing carter (m = 3.980 kg) and the labyrinth sleeve (m = 0.249 kg) contribute to the setup dynamics, since the labyrinth sealing is fixed on rigid parts of the wind tunnel test section.

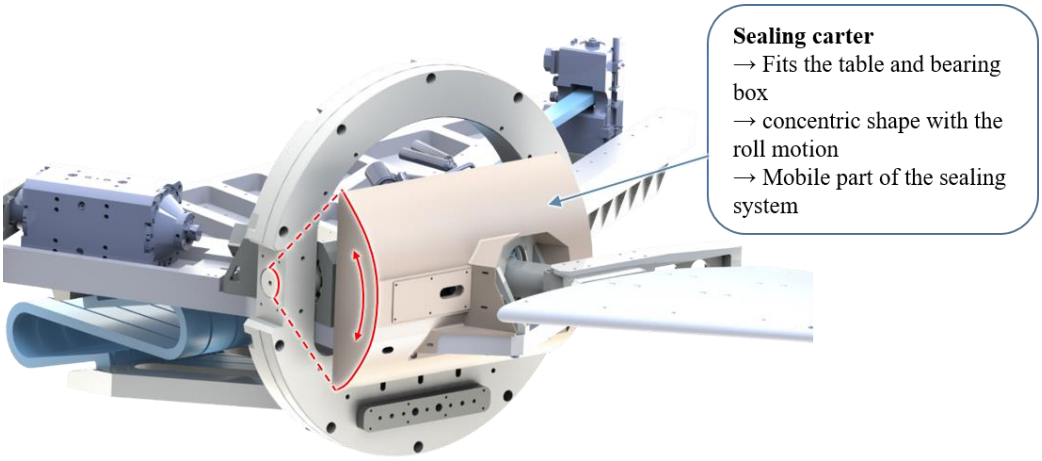

Figure 2-3 Dynamic part of the sealing system

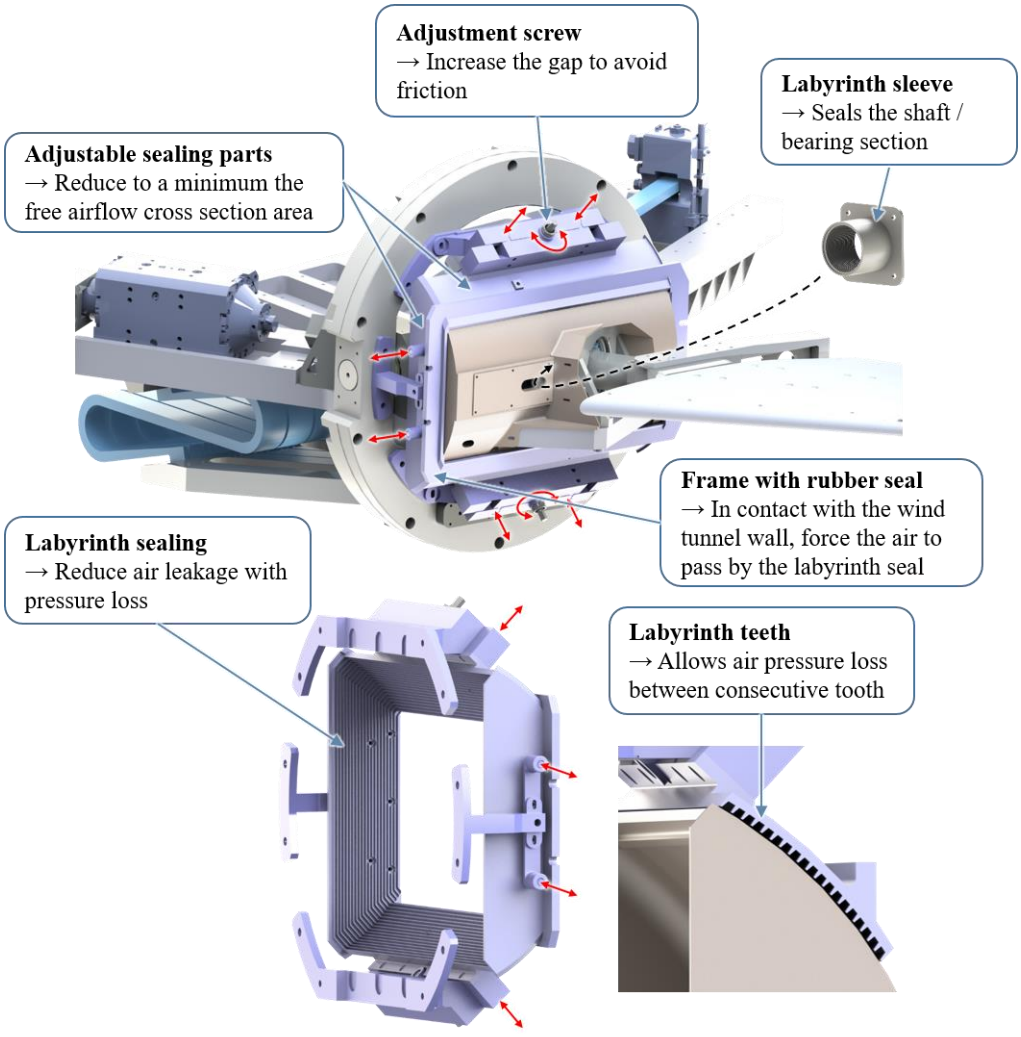

Figure 2-4 Static parts of the sealing system

2.2.2 Additional modifications

In addition to the main solution, a second layer of improvements have been implemented and are presented in Figure 2-5.

First, the fuselage window has been optimized using measured 2016 model motion to reduce the cross section while avoiding contact during flutter onsets. To make the design possible, the clamping system presented in [1] had to be modified to have the smallest footprint at the window opening. Its mass variation is taken into account in the modal analysis process. The new and old fuselage window is displayed in Figure 2-5.

- Previous window cross section → 0.0274 m²
- Current window cross section → 0.0143 m²

Then, top and bottom cutouts on the fuselage were realized to provide an air leakage relocation if needed by simply opening the cutout.

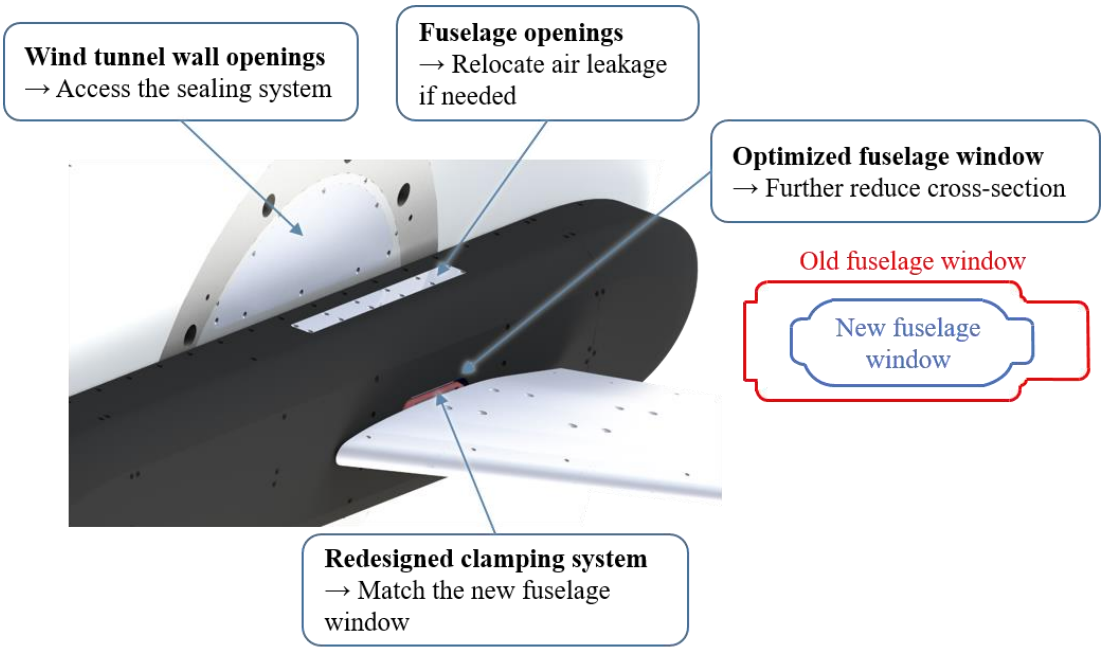

Figure 2-5 Additional setup modifications on the parts inside the test section

The sizing of all the different sealing solutions and setup modifications have been realized following the same principles presented in [1] using finite element models in NASTRAN. They all are safe to operate under the wind tunnel environment conditions. Overall, a 98.5% cross section reduction was achieved considering the freestream sections at the wind tunnel wall opening.

2.3 Model modifications

Four configurations were tested:

- T-2° : -2° yaw angle on the horizontal stabilizer
- T+1° : +1° yaw angle on the horizontal stabilizer
- T-4° : +4° yaw angle on the horizontal stabilizer
- T-2° D-10° : : -2° yaw angle and -10° dihedral angle on the horizontal stabilizer

The following conventions are used:

- Yaw angle increases positively when the leading edge gets closer to the fuselage.
- Dihedral angle increases negatively when the stabilizer tip gets closer to the fuselage.

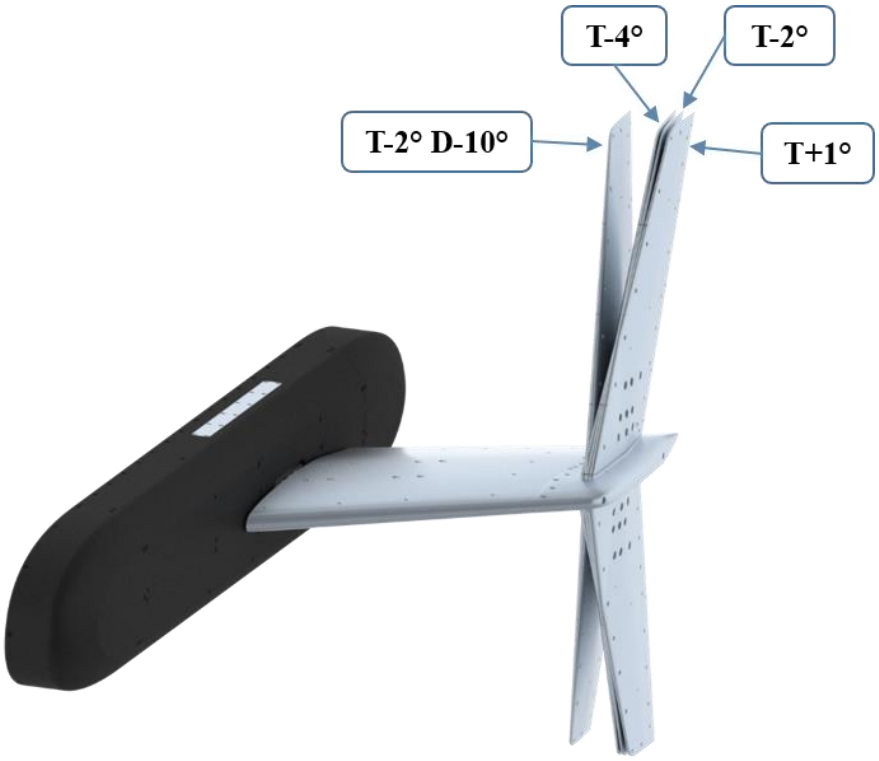

Figure 2-6 Superposition of the 4 T-tail model geometrical configurations for comparison

Additionally, the corner flow region was redesigned by adding a fairing. These modifications required machining the outboard part of the vertical stabilizer with embedded instrumentation. Great care was taken to protect the pressure sensors during the operation, and none of the sensors was damaged in the process. Particular efforts to minimize the mass and inertia modifications were applied, since it could have had a significant impact on the test setup modal behavior. Overall, the mass increase of the T-tail model was of + 0.8 kg (+3%).

Evaluation of the impact of the sealing solution and model modifications on the modal characteristics have been conducted jointly between ONERA and Dassault Aviation using two distinct finite element models of the test setup. Natural frequencies and mode shapes of the first five modes were compared to the original test setup. The analyses are not presented in this paper, but additional mass from the sealing system and the T-tail modifications showed very little impact on the modal parameters of the system. Flutter predictions were performed with DLM and showed that the modified test setup could still enter in the flutter domain inside the S2MA wind tunnel operating conditions.

3 LABORATORY TESTS

3.1 First lab test campaign

After machining and assembly of the new parts of the test setup, everything is mounted on a test rig having the same geometry as the wind tunnel wall. An extensive work not presented here relied on updating the model internal sensors connectors to the new ONERA data acquisition system. The model got reopened and more than 350 sensors were inspected and tested. Laboratory testing focused on the T-2° configuration. Lab testing is a necessary phase before wind tunnel test to check the static and dynamic structural behavior of the model, and the operational capability of every subsystem.

Figure 3-1 Assembled sealing system

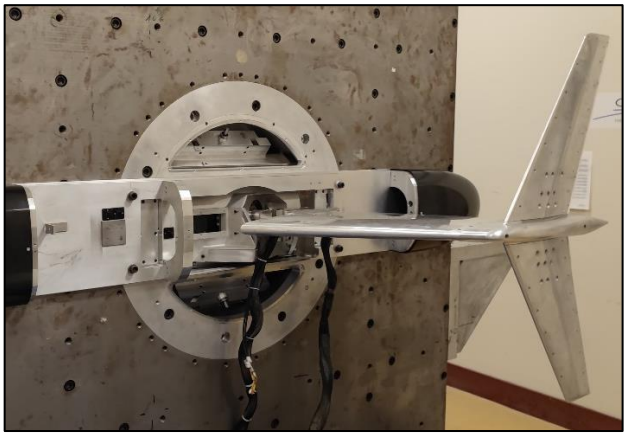

Figure 3-2 T-2° tail model mounted on the lab wall

3.1.1 Ground vibration testing

Ground vibration testing are used to identify the modal characteristics of the model. Excitations of the mock-up are performed using a 45N shaker at strategic locations, where an example can be observed in Figure 3-3. The analysis focused on the first five modes of the model, varying excitation levels, excitation signals and excitation points. Various mechanical configuration parameters of the setup were tested, including torsion beam length, additional masses and safety triggering. Both flutter and pressure mechanical configurations were tested, with the embedded hydraulic actuator. Modal analysis is performed on the sensors time signals (mainly force cell, accelerometers and strain gages) to identify the modal parameters in all the configurations described above.

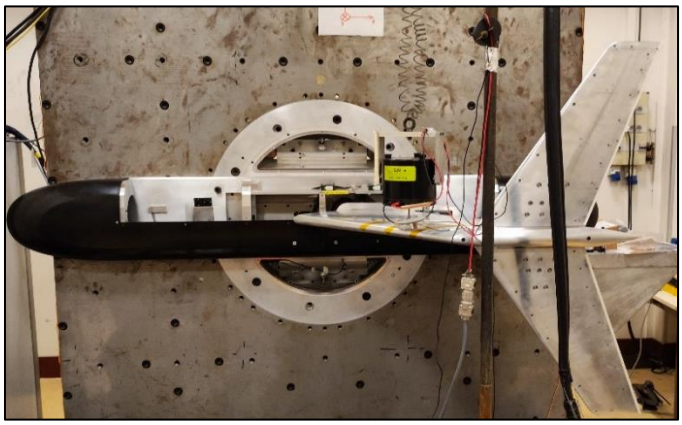

Figure 3-3 Ground vibration tests in laboratory

An example of the frequency response function (FRF) obtained is presented in Figure 3-4. Five modes of the model were identified and presented the linear behavior wanted for the purpose of this study, giving a first indication of a frictionless test setup. Higher energy levels were applied to increase the model motion and seek for contact. No contact could be observed in any of these runs.

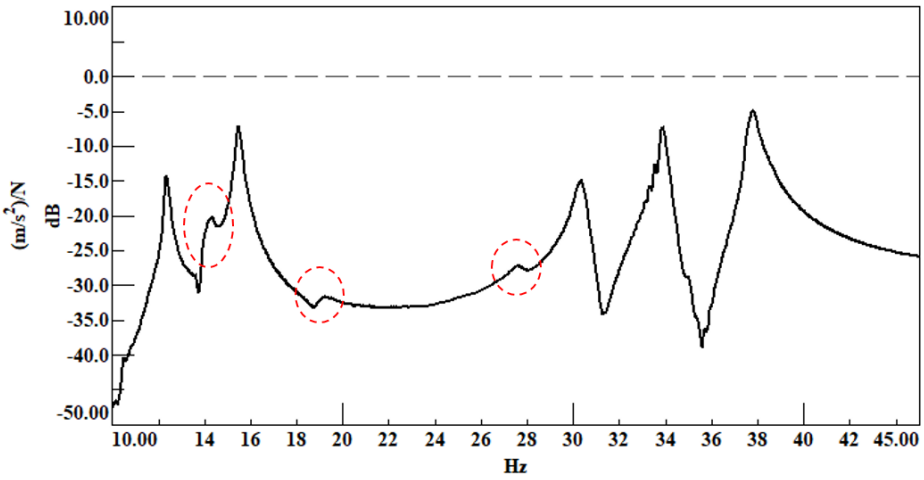

Figure 3-4 Frequency response function from firsts lab testing

Additional modes circled in Figure 3-4 were also observed. First thought linked these new modes to the modifications on the setup. After further investigations and the addition of 30 accelerometers to the setup, we concluded that these 3 modes were related to the test rig that was modified for the purpose of this lab testing, which had not been modified in 2016. The decision to validate the setup was made since these 3 additional modes would not be present in the wind tunnel facility, having boundary conditions cleaner than on the test rig.

Energy variations were used to build impedance curves and identify frequencies, damping, generalized masses and mode shapes of the first five modes at high energy levels. Impedance curves presented in Figure 3-5 at several torsion beam lengths were made to identify the optimal torsion beam length for the test to have flutter in the targeted aerodynamic domain.

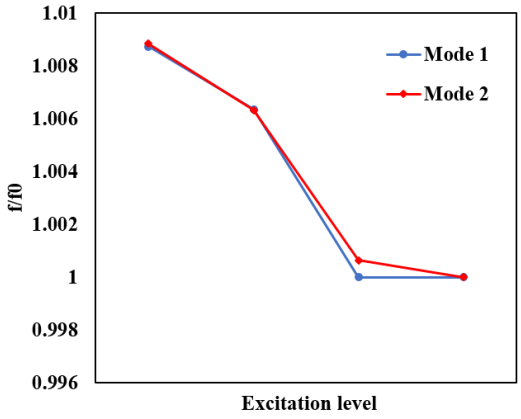

Figure 3-5 Impedance curves for the first two modes

3.1.2 Static tests

Static tests were also performed to check if we kept the structural linear behavior of the model, and see if contact could occur on a highly deformed model. Aerodynamic loads are simulated both on the vertical stabilizer and the two horizontal stabilizers using pneumatic actuators. Force cells measure the input force and optical sensors measure the response on the structure. Figure 3-6 and Figure 3-7 present the experimental setup.

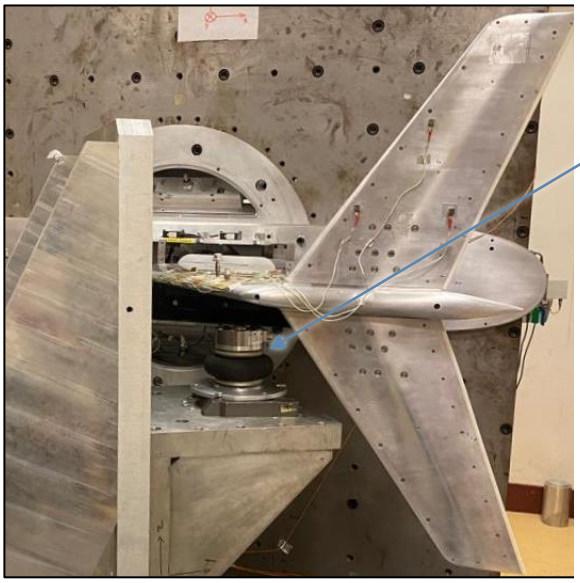

Figure 3-6 Static tests on the horizontal stabilizer

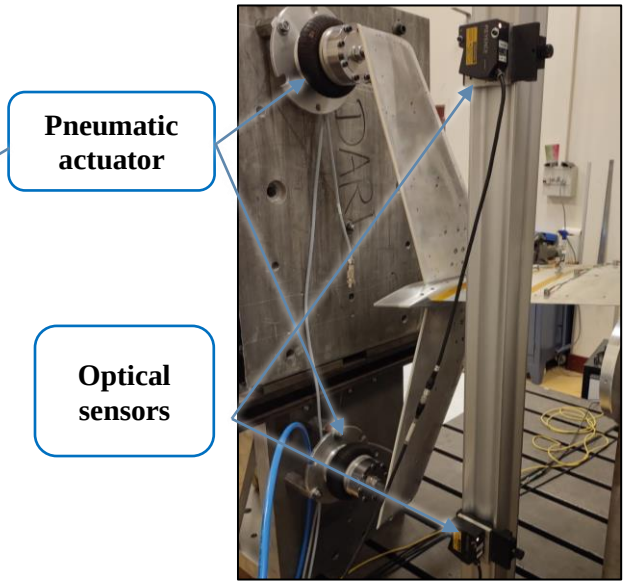

Figure 3-7 Static tests on the vertical stabilizers

Forces up to 3000 N were applied on the vertical stabilizer. We observe a linear evolution of the displacement with small hysteresis. On the horizontal stabilizers, forces of 1000 N were applied and both displacements present a linear evolution with the amount of force. Results are comparable to the ones from 2016, showing that the test setup has a similar behavior.

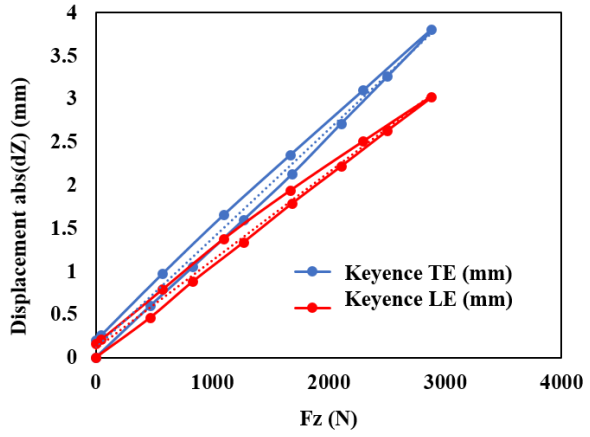

Figure 3-8 Static tests on vertical stabilizer

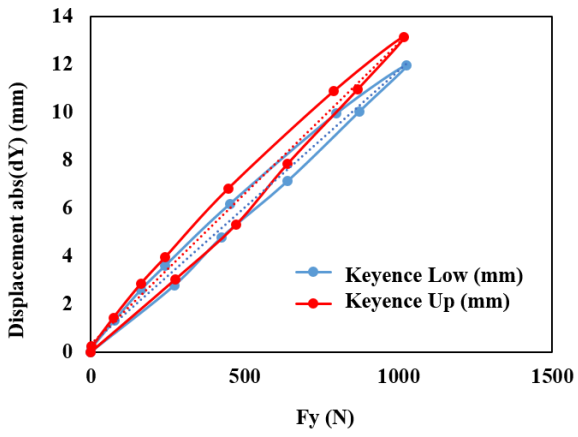

Figure 3-9 Static test on the horizontal stabilizers

3.2 Second lab test campaign

A second run of modal identification is mandatory once the test setup is installed in the wind tunnel. Boundary conditions are important and play a non-negligible role in the modal parameters. Figure 3-10 shows a picture of the ground vibration test, where four additional measurement lines were added externally with 2 accelerometers each to increase the measurement density and accuracy of the modal parameters identification, particularly the modes shape. 3D printed shapes were designed to have the external accelerometer measurements directly in the global coordinate system.

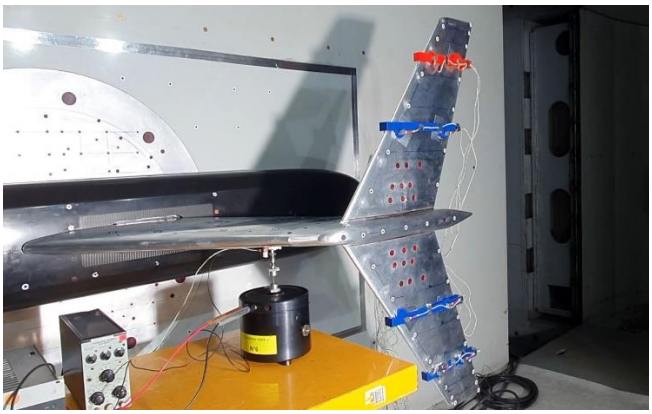

Figure 3-10 Ground vibration test inside the wind tunnel test section

Measured FRF from an accelerometer on the upper stabilizer are presented below, where comparisons are made between the 2016 test inside the WT, and 2022 results inside the WT and on the test rig. Additional modes observed on the test rig are no longer present in the WT environment, validating the conclusion that these additional modes were indeed test rig modes. We also observe a drop in the first two modes comparing the 2016 and 2022 results. This was expected since the mass added by the sealing system and the new model geometry tend to decrease the natural frequencies. Modal parameters and the firsts mode shapes are given in Table 1 for the T-2° configuration.

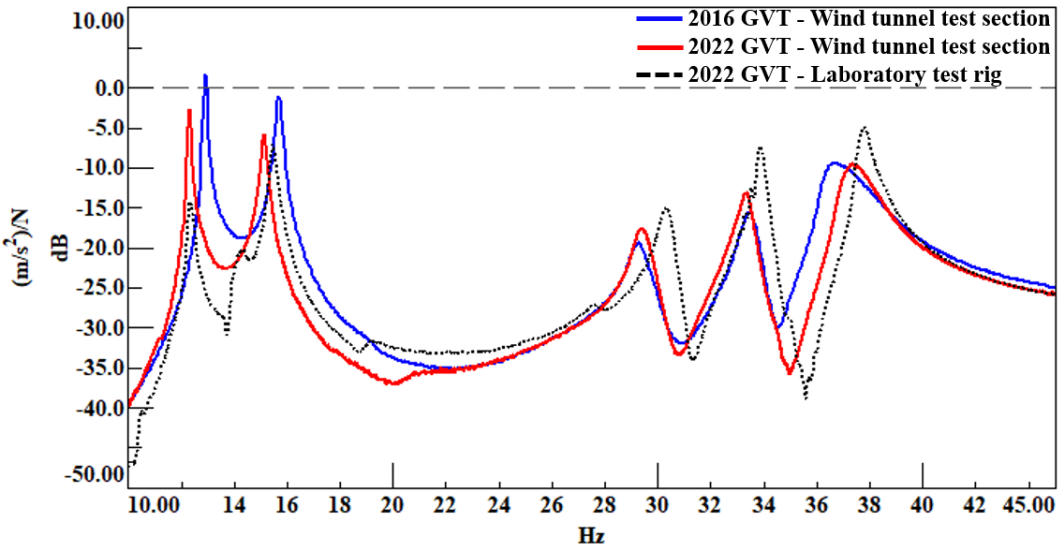

Figure 3-11 FRF comparisons between 2016 and 2022 tests

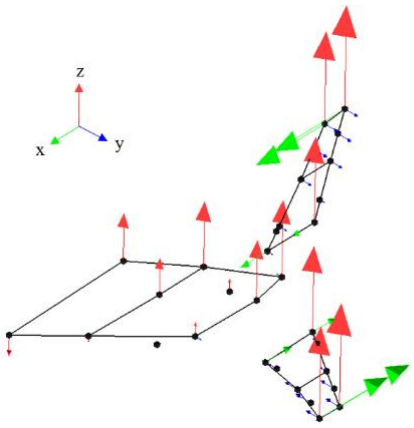

Figure 3-12 First mode shape

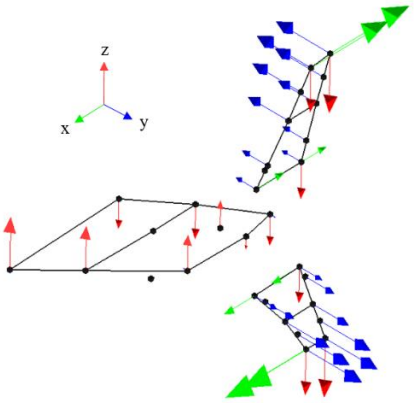

Figure 3-13 Second mode shape

Table 1 Modal properties for the T-2° geometrical configuration

Mode n°	Natural frequency	Damping	Generalized mass
1	12.32 Hz	0.43%	15.35 kg.m²
2	15.15 Hz	0.81%	13.84 kg.m²
3	29.41 Hz	0.93%	9.14 kg.m²
4	33.32 Hz	1.11%	6.59 kg.m²
5	37.31 Hz	0.92%	9.48 kg.m²

Taking into account the measured data from all displacement sensors, the group of measured FRF was used in a modal identification process with PolyMAX.

Modal identifications for each configuration are mandatory for the completion of flutter simulations using high-fidelity software that will be presented in a companion paper [2]. Additionally, these values are important for Dassault Aviation to tune the finite element model, and perform flutter simulation with numerical modes. During the wind tunnel test campaign, ground vibration tests are performed before and after each model geometrical configuration modification. This serves two purposes, get the modal parameters for each configuration, and assess the structural integrity of the setup verifying that no damage occurred on each configuration during flutter onsets.

Figure 3-12 and Figure 3-13 show the two first modal shapes discretized on the accelerometer meshing. The first mode being a roll of the table where flexibility comes from the S-beams, all accelerometers in the Z direction are in phase, except the ones on the other side of the nodal line located close to the root of the vertical stabilizer. The same observation is made for the second mode, the pitch of the model given by the flexibility of the torsion beam lead to a 180° phase shift between leading and trailing edge Z accelerometers. These two modes participates in the flutter instability coupling together.

4 WIND TUNNEL TESTS

After 4 weeks of preparation outside the test section and one week of installation, the mock-up can finally be tested in transonic conditions. The test started with the T-2° configuration on which most of the lab testing was performed. A first assessment of the efficiency of the sealing condition had to be performed before going on with the test matrix. Followed the T+1° and T-4° configurations, with the dihedral effect tested at the end. Seven Mach numbers were targeted in the test matrix going from M=0.7 for subsonic and low Reynolds, up to M=0.925 for high transonic flow with transonic dip phenomenon.

Figure 4-1 T-tail model (T-2°) inside the S2MA transonic wind tunnel

4.1 Methodology

More than 350 channels are recorded during the test, where a specific software presented in [1] ensures synchronization between the aeroelastic DAQ systems and the wind tunnel DAQ systems. 258 pressure sensors are spread over 10 chord lines on the mock-up as presented in Figure 4-2. Region of high-pressure sensor density are the upper side of the vertical stabilizer, and the side facing the fuselage on the horizontal stabilizer. Both a real-time controller and an analog controller, analyzing the acceleration signals from sensors on the horizontal and vertical stabilizer, control the safety system. In addition, markers are positioned on the model and the wall to track model deformation using two cameras. Model deformation measurement (MDM) is used for static and dynamic pressure tests as well as flutter onsets. For test sequence optimization and due to the time needed for the image transfer from the cameras to the SSD, MDM dynamic measurements are limited to 7s at 120 Hz. During flutter onsets, the safety system signal is used to trigger the cameras, which record the last 7s from the trigger. Wool tufts are installed at the root of the model to have direct visualization of the streamlines, and see if we still observe perturbed aerodynamics due to air leakage.

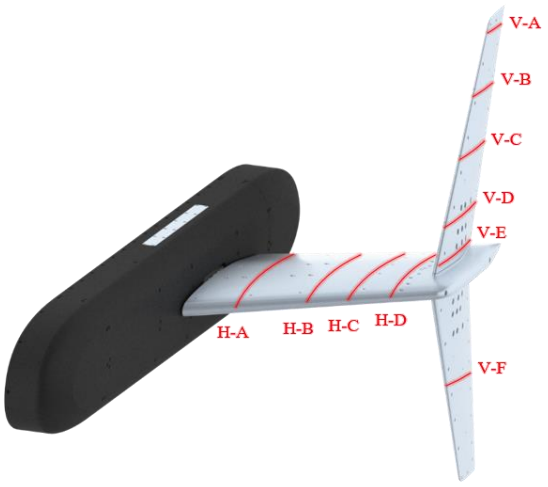

Figure 4-2 Unsteady pressure measurement lines location

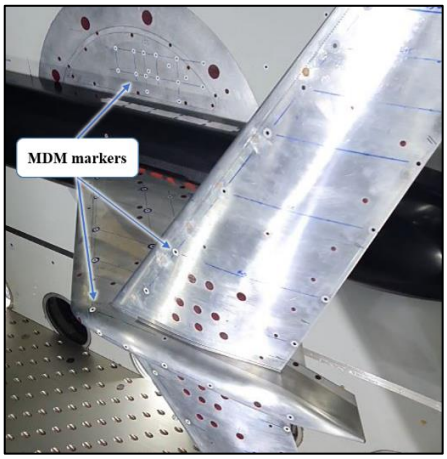

Figure 4-3 Model Deformation Measurement (MDM) markers

4.2 Sealing system assessment

Firsts rotations were dedicated to the sealing system assessment. Pressure mechanical configuration is set to study the aerodynamics at different angles of attack and Mach number. The first direct indicator of the flow quality are the wool tufts, observable through security cameras. Figure 4-4 presents two screenshots of the model root at M=0.7 from 2016 and 2022. Aerodynamics seems much better on the 2022 test with less perturbed wool tufts. Some streamlines are perturbed close to the fuselage window, but nothing compares with the 2016 figure where 45° angle streamlines are observed near the window. Additionally, the airflow perturbation from 2016 covers a much greater area than what is observed in 2022. Thus, effects on the mock-up aeroelastic behavior should be drastically reduced. The same observations are made at higher Mach numbers, and we see no difference varying the angle of attack of the mockup.

The effect of upper and lower fuselage openings was also investigated, but had no measured aerodynamic impact, reinforcing the conclusion of the effectiveness of the sealing system. Due to time constraints and the necessity to maximize the data production from the test, gaps in the sealing system parts were not modified to avoid contacts during flutter onsets.

To try to further investigate the phenomenon, rotations with aluminum tape between the model root and the fuselage, sealing completely the model/fuselage junction was conducted. Little improvement on the wool tufts perturbation was observed, but this configuration does not only bypass the leakage effect, it also gets rid of the complexity of the geometry at the root of the model. This leads to a much simpler representation, without a 1cm gap between the fuselage and the model, an airflow deviation due to the shaft, and perturbations due to the window geometry itself.

The second indicator used to evaluate the sealing system effectiveness is the first pressure sensor line (H-A), used to compute RMS/Q0 and Kp values (difference between the average pressure and the WT static pressure normalized by the dynamic pressure) presented in Figure 4-5. The Results comparison from the two tests is presented for different angles of attack at M=0.85. For each angle of attack, RMS comparison shows high discrepancies close to the trailing edge where aerodynamics was the most perturbed between the 2016 and 2022 results. Looking at the Kp results, the differences are less obvious. Slightly higher values are observed in the 2016 results, which could indicate the end of a flow separation at this span location. We have to recall that this

pressure sensor line is not directly located at the model root, and that only the edge of the identified leakage region was crossing the pressure measurement line. This could explain why some sensibility of flutter onset was observed in 2016 depending on the sealing of the fuselage window. From these observations, the aerodynamic improvement from the designed sealing system was validated.

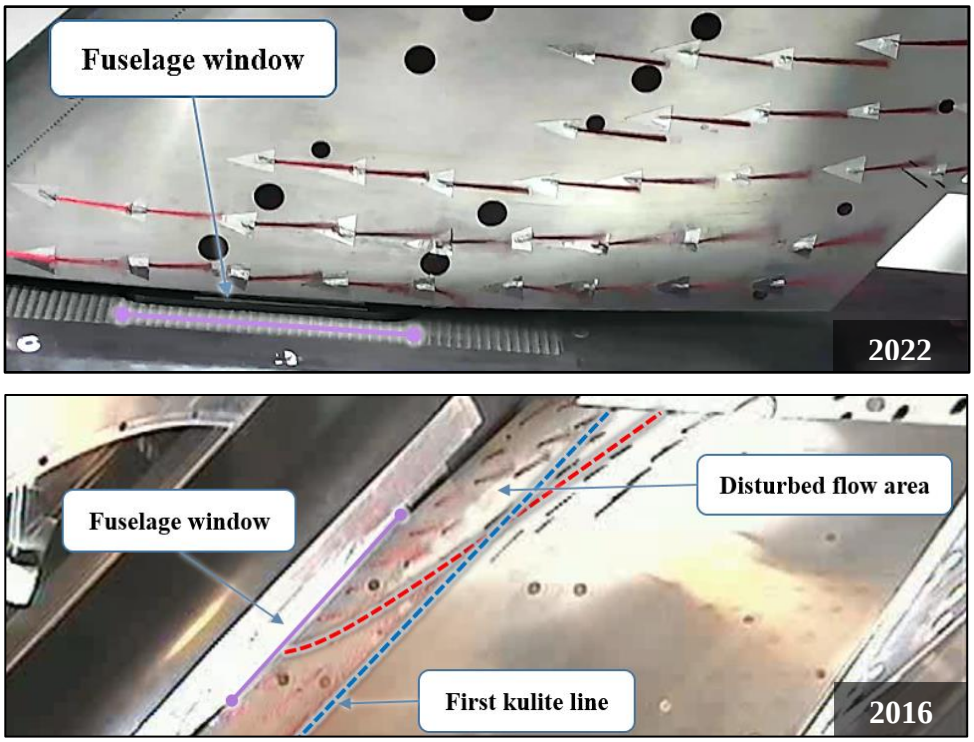

Figure 4-4 Wool tuft comparison between 2016 test and 2022, T-2°, M=0.7, Pi=1bar, AoA=0°

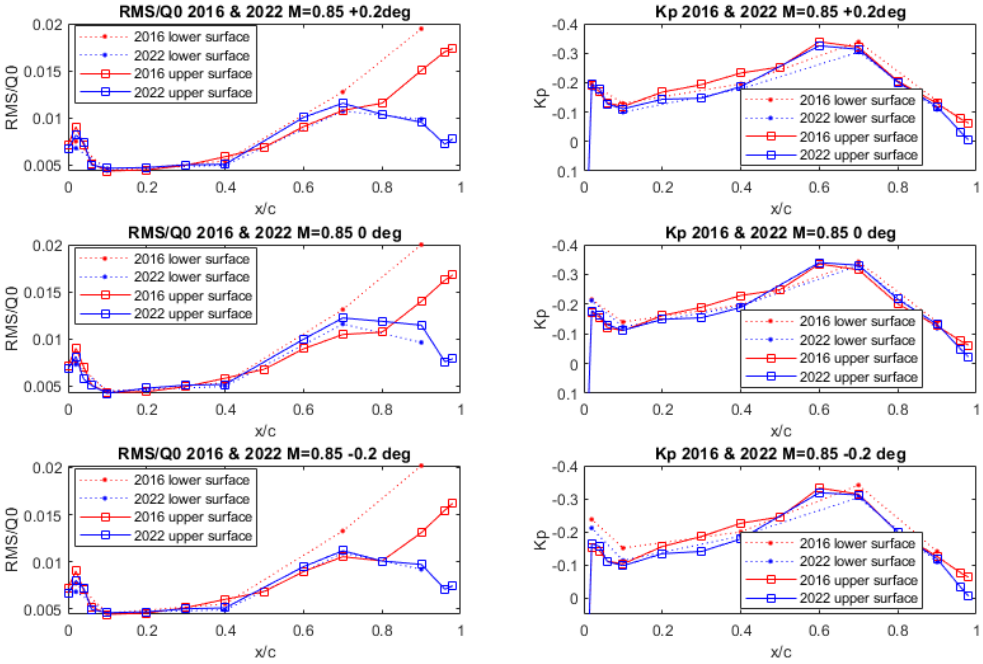

Figure 4-5 H-A pressure sensor line measurement: RMS/Q0 and Kp values, M=0.85

4.3 Pressure tests

Objectives of the pressure tests are the identification of steady and unsteady aerodynamics, with variations of pitch angle, dynamic motion frequency and amplitude, wind tunnel pressure and Mach number. Dynamic pitch amplitude of 0.2° and 0.5° are tested at excitation frequencies of 5Hz, 15Hz, and 30Hz. Pressure effects are also introduced with some measurements performed at 1.5 bar instead of 1 bar.

A prerequisite for pressure tests is the knowledge of the dynamic behavior of each pressure configuration to avoid having excitation frequencies close to the natural frequencies of the model.

4.3.1 Steady aerodynamics

The 10 pressure measurement lines spread on the model give a good representation of the aerodynamic phenomena occurring on the model. Figure 4-6 presents the angle of incidence effects at M=0.85 for the T-2° yaw angle configuration on the two pressure sensor lines near the corner flow region. We can see that for this Mach number, no flow separation is observed. A shock is measured both on the horizontal and vertical stabilizer at the same region, which seems to be lightly affected by small variation of angle of attack.

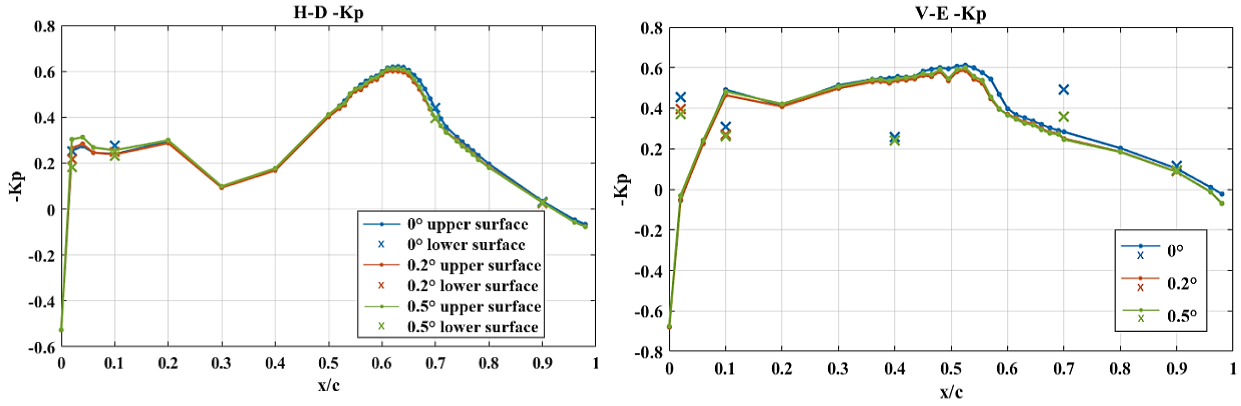

Figure 4-6 Static angle of incidence effect on the T-2° configuration at M=0.85

Mach effects are presented for the T+1° geometrical configuration at a static angle of attack of 0° in Figure 4-7. The aerodynamics in the corner region show as expected high variations depending on the Mach number. From a subsonic flow at M=0.7 where no shock appears, transonic effects then take place at M=0.85 and M=0.925 with a shock location moving towards the trailing edge with increasing Mach number. For both Mach numbers, the shock location seems to be at the same location on the vertical and horizontal tail plane. Flow separation seems to occur at M=0.925 in the corner region looking at the trailing edge pressure sensors. Increasing the Mach number, a second shock appears closer to the leading edge. Geometrical configuration effects are presented in Figure 4-8 at M=0.85 and AoA=0°, with a focus still on the corner flow region and an additional line on the upper part of the horizontal stabilizer. With increasing yaw angle, airflow in the corner region is accelerated for the same aerodynamic condition. A stronger shock is observed for the T+1° configuration and for the T-2°. Yaw angle variations can also be noticed on the V-C line, with a higher pressure differential plateau with yaw angle increase. V-E pressure sensor line also show a shock happening closer to the trailing edge on the T+1° configuration which is not observed on the T-4° yaw angle. The observed bump on the low pressure data region before the shock of

the T+1° configuration can indicate interactions between the intersecting planes with shock propagation.

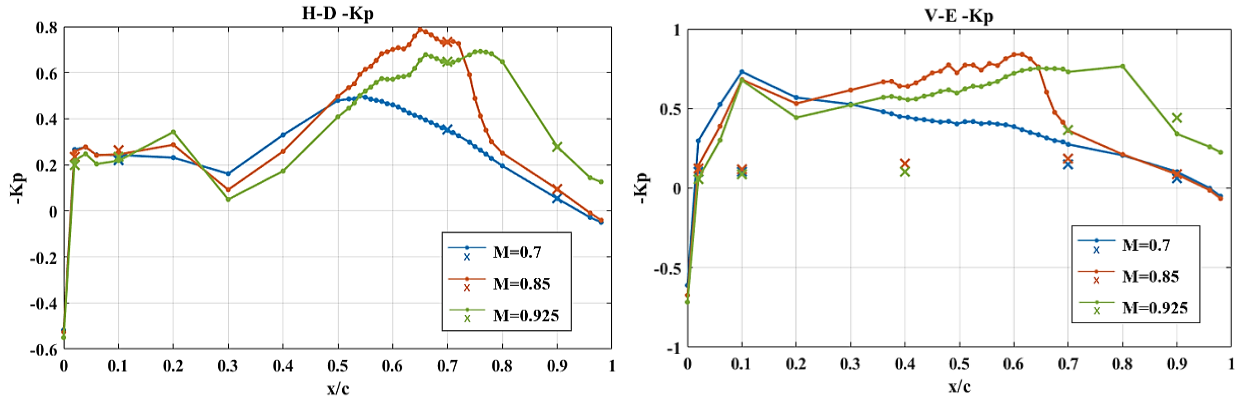

Figure 4-7 Mach effect on static pressure test of the T+1° configuration at AoA=0°

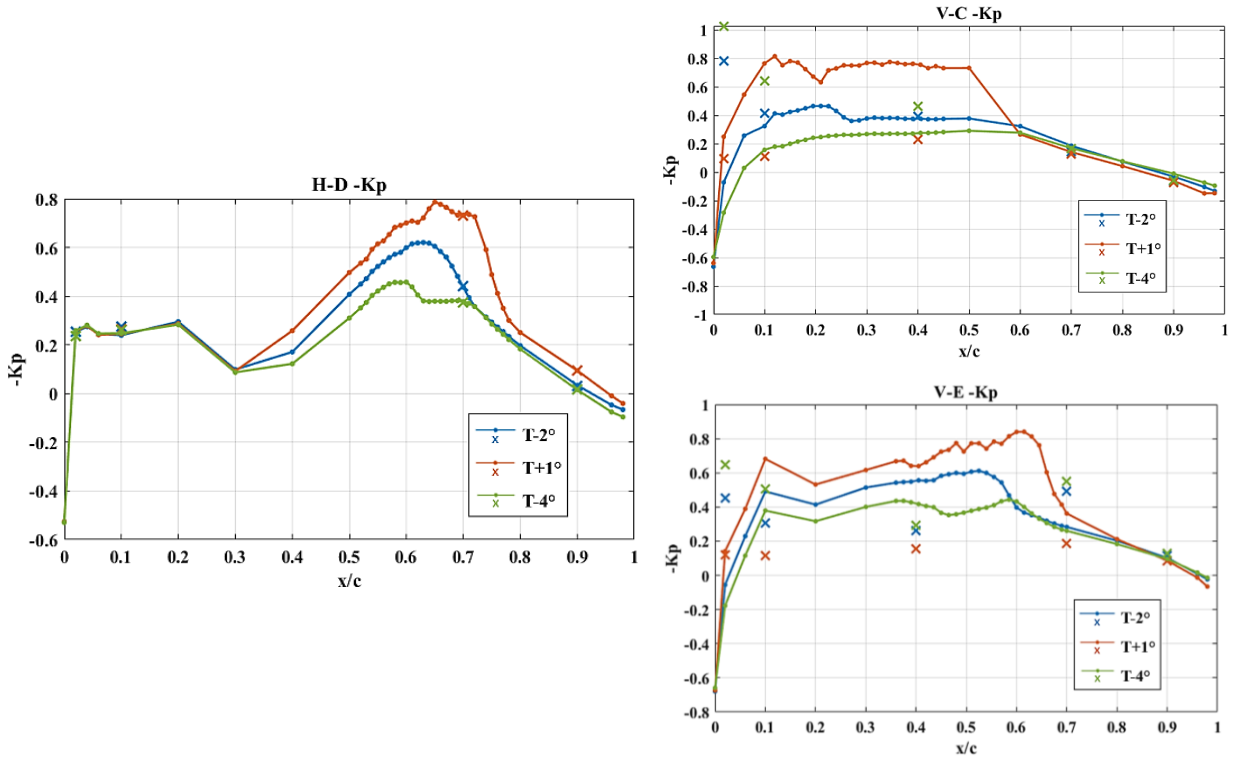

Figure 4-8 Static configuration effect at M=0.85 and AoA=0°

MDM measurements allow for both static and pressure tests to have direct measurements of the model deformation at the marker locations. Figure 4-9 presents the interpolation of the marker on a panel mesh, for the T-4° geometrical configuration during static tests at different Mach numbers. The undeformed mesh is represented in gray, the interpolated mesh at M=0.7 is presented in red and the interpolation at M=0.85 is presented in blue. For increasing Mach number, aerodynamic forces tend to deform the model in the direction of the span, which was expected for a negative yaw angle T-tail configuration. Only a 3.6mm static displacement in the Y direction was observed

for this configuration between the undeformed model and the model at M=0.85. Other geometrical configurations present smaller static deflections since they have smaller yaw angle values.

These little displacements observed give additional credibility to the hypothesis of an undeformed model taken for numerical simulations. Additionally, deformations during dynamic excitations of the mock-up were still in the order of magnitude of a few millimeter, and the undeformed hypothesis is still valid under dynamic motion. An interpolation over the CFD mesh could be achieved to study the sensitivity of the results to a few millimeters displacements on the model horizontal and vertical stabilizers. However, deformations are much less important than the ones presented in [3], since the U configurations is not balanced regarding the loads, and tend to deflect the vertical stabilizer as well, increasing the horizontal stabilizer displacement. Results in CFD computations taking into account model deflection would not present as much differences for the T-tail application.

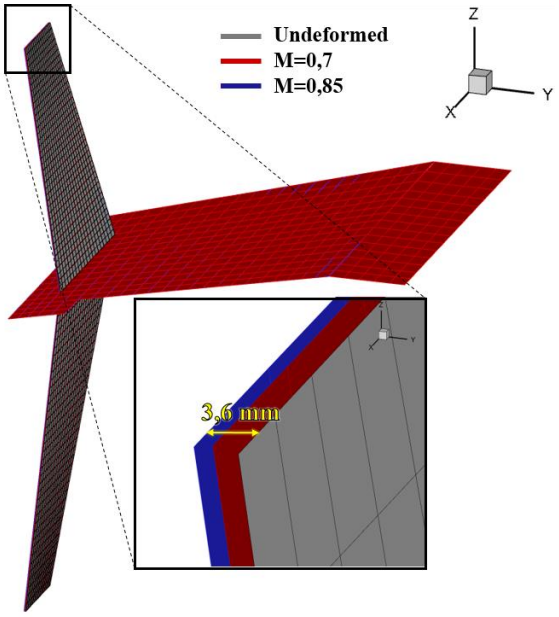

Figure 4-9 Model deformation for the T-4° configuration at AoA=0°

4.3.2 Unsteady aerodynamics

Thanks to the hydraulic actuator, dynamic pressure tests can be performed for unsteady aerodynamic identification. The shaft of the model is clamped to the actuator, and a servo controller introduce a static or dynamic pitch angle on the model. Three ways are available to determine the model reference motion. First, an RVDT rotation sensor located on the hydraulic actuator gives direct information on the angular motion. Then, two optical sensors are positioned inside the fuselage and measure the distances of two specific points of the shaft. An angle can be deduced from this measurement for both static and dynamic tests. Finally, the two first row accelerometers can be used to identify the angular motion of the model. Accelerometers are less accurate at low frequencies due to their cutoff, and RVDT measurements suffer from the distance to the model, which can cause phase latency with the actual model motion. Differences in the comparison of numerical and experimental results could come from the phase reference taken,

depending on the sensor used for the experimental data post processing. These phase differences can be used as an uncertainty range when comparing numerical results with the experiment.

Geometrical configuration effects for 0.2° pitch motion dynamic excitation at 15Hz at M=0.85 are presented in Figure 4-10. Harmonic pressure coefficients are the measured FRF from pressure sensors evaluated at the excitation frequency, and normalized by the WT dynamic pressure. The shock intensity and position variations are here again noticed in the corner flow region on the real part of the pressure coefficient. Differences are also observed on the imaginary parts, with a zero crossing located at 10% chord for all the geometrical configurations. Imaginary parts for the T+1° model are higher than for other configurations at the shock location.

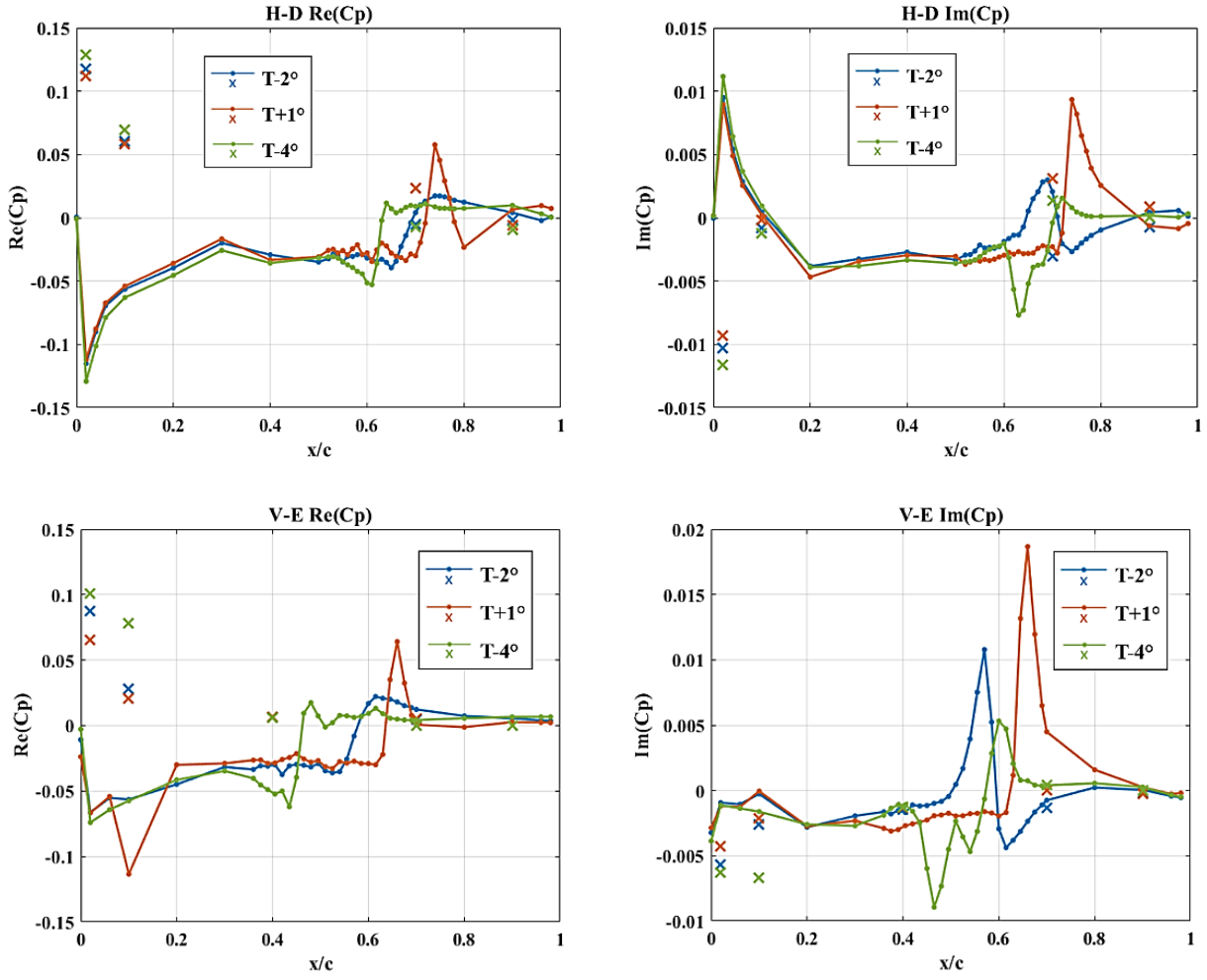

Figure 4-10 Dynamic configuration effects at f=15Hz M=0.85 and AoA=±0.2°

Frequency effects on the T-2° configuration are presented in Figure 4-11 at M=0.85. A small influence of excitation frequency is observed on the real parts, but we notice an increase in the imaginary part participation at higher excitation frequency. We can deduce from that an increase in the pressure variations out of phase with the model displacement.

Additional analysis and comparison with model prediction results will be provided in [2].

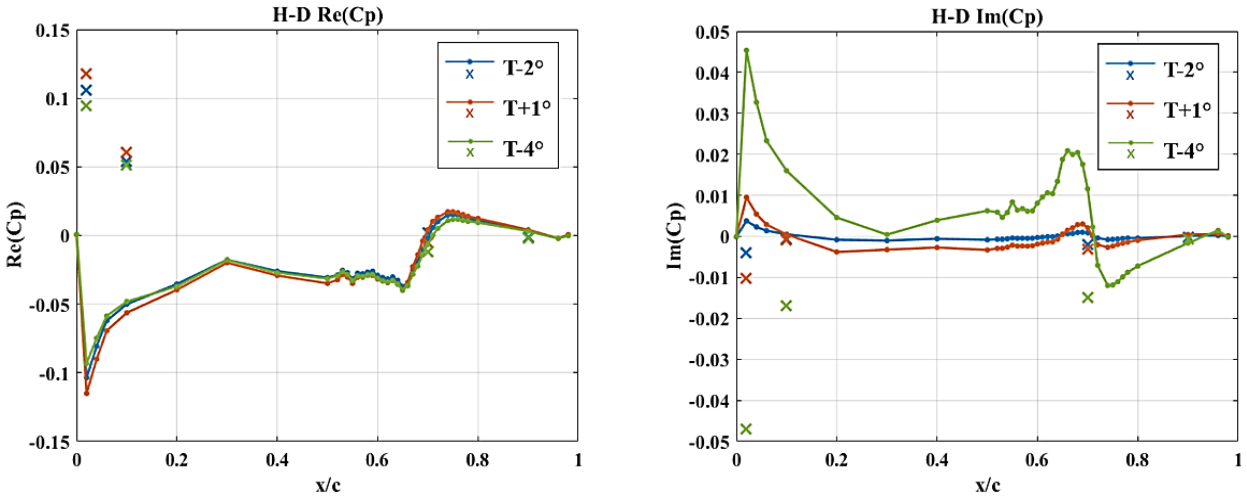

Figure 4-11 Frequency effects on the T-2° configuration at M=0.85 and AoA=±0.2°

4.4 Flutter tests

Flutter tests started first with an identification of an ideal torsion beam length that could lead to flutter onsets inside the WT operating domain for all model geometrical configurations. The tested lengths were [1000 1060 1090 1120] mm and the selected length for the entire campaign was 1060mm. For each configuration and at fixed Mach number, WT stagnation pressure is increased until the start of the aeroelastic instability and the security trigger. We can deduce the flutter critical pressure, being our flutter index, for each aerodynamic and geometric configuration. During the test, a high repeatability of the results was obtained with a repeatability of ± 0.01 bar, which was not achieved in 2016. This gives better trust in the obtained results and participates showing that the sealing system and the model modification highly improved the quality of the experimental results.

The main outcome is presented in Figure 4-12 where yaw and dihedral angle effects on the aeroelastic behavior of the T-tail model are highlighted. The stabilizing effect of the negative dihedral angle is observed, with a shift of the critical pressure 0.6 bar higher than for other configurations at M=0.8. Flutter was not observed at M=0.7 as we reached the boundary of WT test operating conditions in terms of available stagnation pressure. Yaw angle effects are also observed, where a yaw angle decrease tend to destabilize the mock-up. This effect is consistent at each Mach number. Transonic dip were measured for the T+1° and T-2° configurations, occurring around M=0.875 and M=0.9. Transonic dip on the T-4° is not clearly visible and is probably not yet reached. Comparisons with the numerical predictions are presented in a companion paper [2].

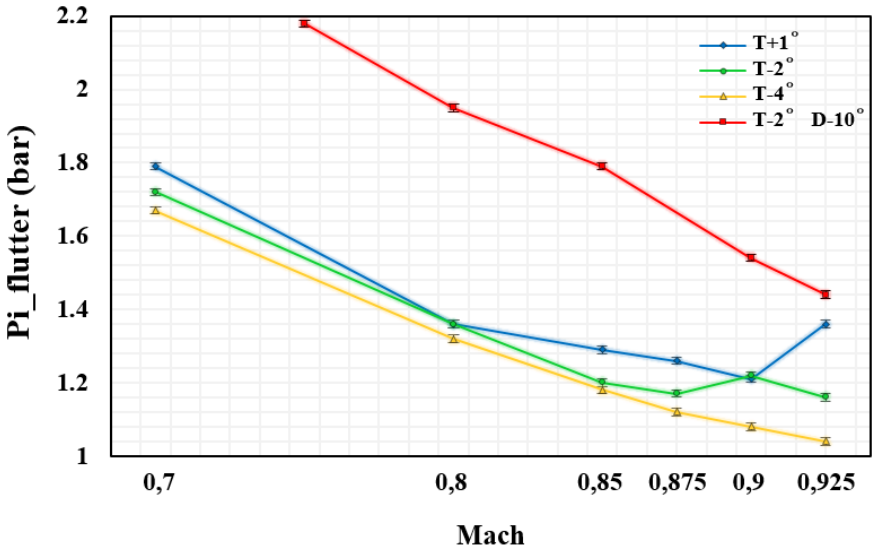

Figure 4-12 Flutter critical pressure for each T-tail model geometry

Flutter critical pressures being identified, flutter curves can be obtained from modal identification at several stabilized pressure points below the flutter critical pressure. The hydraulic actuator on the table with the unbalanced mass is used to excite the test setup with white noise to improve the levels of aeroelastic response of the structure. Figure 4-13 presents the identified flutter curves for the T+1° configuration at M = 0.875. With increasing participation of generalized aerodynamic forces due to pressure increase in the aeroelastic equation of the model, pitch and roll mode frequencies get closer to each other, up to a point where modal interaction leads to a drop in damping of the first mode. The point of zero damping corresponds to the critical pressure. The advantage given by the onboard security system is that not only true flutter onsets can be measured, but flutter sharpness which is of high importance can also be studied. Stabilized points at a pressure very close to the critical pressure can be safely measured for a long time without the risk of damaging the setup.

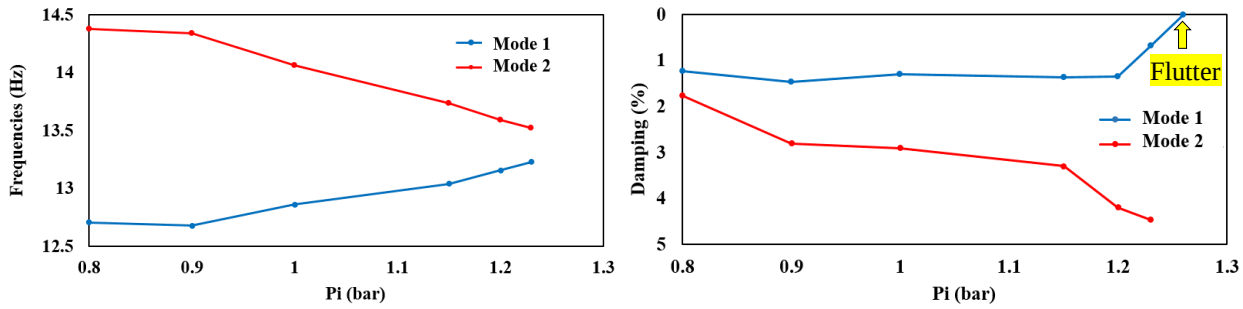

Figure 4-13 Flutter curves for the T+1° mock-up, evolution of modal frequencies and damping with WT pressure

Model displacement during flutter onset can be projected on the mode shapes. Here, a projection of the deplacement on the two first mode shapes identified during the ground vibration testing shows the increase of the participation factor of the first mode entering flutter with a very small

damping. Then coupling occurs and participation of the second mode increases before the trigger of the safety system.

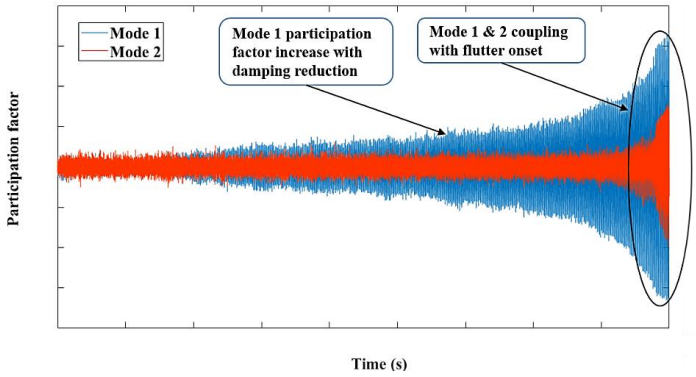

Figure 4-14 T-tail model displacement projection on the two first mode shapes

During flutter onsets, the inductive sensor measuring the sealing system parts gap was monitored to ensure no contact occurrence. Typical results obtained are presented in Figure 4-15 and Figure 4-16, where the maximum gap distance variation was around 0.1 mm. The sealing system design respects accurately the setup degrees of freedom, and amplitudes of model deformation observed during the WT test campaign do not risk being impacted by the system.

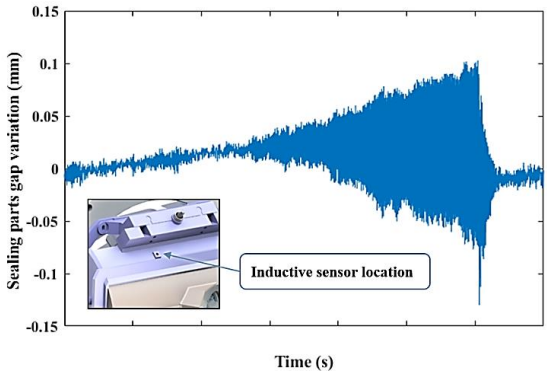

Figure 4-15 Sealing system gap variation during flutter onset

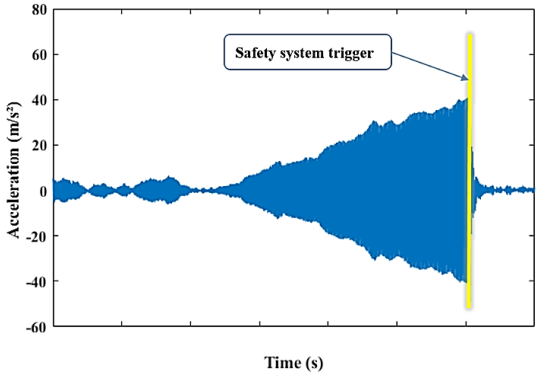

Figure 4-16 Accelerometer response during flutter onset

5 CONCLUSIONS

This test campaign in the ONERA S2MA wind tunnel is the culmination of a 3-year research program, where more than 350 runs were measured with many parameter variations including Mach and Reynolds number, pitch angle, excitation frequency and model yaw angles. More than 70 flutter onsets were recorded safely with high repeatability on all of the four geometrical model configurations, demonstrating ONERA expertise in terms of flutter testing. The test exhibited aerodynamic effects from subsonic up to high transonic domains for complex intersecting surfaces, giving a rich database to understand aeroelastic phenomena occurring on T-tail configurations. Steady aerodynamic measurements presented important differences in the shock intensity between the different yaw angle configurations in the corner flow region. Optical model deformation measurements gave additional information on the model deformation under different aerodynamic conditions. CFD computations on the deformed model could be investigated to evaluate the influence of small deformations under aerodynamic loadings. Harmonic pressure data will allow

the evaluation of the performance of unsteady aerodynamic simulations for complex configurations.

The sealing solution selected to prevent leakage through the cross-section of fixed and moving parts of the setup proved its efficiency during the entire test campaign. A clear improvement of the aerodynamics at the root of the mock-up was observed and without any influence on the dynamic behavior of the setup. Even during flutter onsets, with high pitch and roll motion amplitudes, the sealing system did not seem to impact negatively the results, either for pressure or flutter tests. On the other hand, a compromise between experimental necessities and simulation complexity has to be taken for accurate results comparisons. Even without leakage, aerodynamic at the root of the model is still complex due to the gap between the fuselage and the model root, necessary for model angular motion. The model shaft also deviates airflow on the upper and lower side of the model which can deteriorate model root aerodynamics. CFD simulations including these elements would help to evaluate the influence of these setup characteristics on the measured results, and give further fidelity to the experiment modeling.

A great teamwork between ONERA and Dassault Aviation has to be highlighted. The knowledge acquired during the project duration will be reinvested in future research programs, especially for the topics related to the investigation of new aeroelastic phenomena present in future aircraft configurations. The presented paper shows that flutter behaviors on various model geometrical configurations can successfully be evaluated through wind tunnel test campaign, with high accuracy and high density of measured data. The constant improvement of experimental techniques and knowledge lead more and more to higher quality databases, and help the assessment of CFD software on new complex configurations.

REFERENCES

[1] Geeraert A., Lepage A., Stephani P., Feldmann D., Häberli W., Wind tunnel flutter test of a U-tail configuration – Part1: Model design and testing", IFASD 2017, Como – Italy

[2] Dequand S., Lanari V., "T-tail transonic flutter wind tunnel test – Part 2: Numerical restitution", IFASD 2024, Den Haag

[3] Mamelle H., Broux G., Garrigues E., "Wind tunnel flutter tests of a U-tail configuration Part 2: experimental and numerical results", IFASD 2017, Como – Italy

[4] Szymanski A., Dykas S., "Evaluation of leakage through labyrinth seals with analytical models", TASK Q. Sci. Bull. Cent. Informatics - Tricity Acad. Supercomput. Netw., 2019.

ACKNOWLEDGMENTS

This work has been funded within the frame of the Joint Technology Initiative JTI Clean Sky 2, AIRFRAME Integrated Technology Demonstrator platform "AIRFRAME ITD" (contract N. CS2-AIR-GAM-2020-21-04) being part of the Horizon 2020 research and Innovation framework program of the European Commission.

COPYRIGHT STATEMENT